A Kolsky Bar for High-Rate Indentation

D. T. Casem[1] · E. L. Retzlaff[2]

Abstract

A Kolsky Bar for high-rate indentation has been developed. Samples are adhered to the end of the input bar and the indenter is mounted/machined directly on the end of the output bar, in a way that only negligibly affects the output bar's otherwise uniform impedance. When the input pulse reaches the sample, the sample is driven into the output bar and loaded. By properly choosing the lengths and impedances of the bars and striker, the maximum load and loading duration can be reliably controlled. It can furthermore be ensured that the sample is only subjected to a single loading; i.e., the sample is not reloaded due to later stress-wave reverberations in the bars even though momentum trapping is not used. Depending on the sample and desired indentation load, unusually small output bars (less than 2 mm diameter) may be needed. For this reason, the output bar is instrumented with a normal displacement interferometer on the free-end. This provides an accurate measurement of the motion of the indenter tip and the indentation force. The sample face is instrumented with an additional displacement interferometer and these two displacement measurements are used to determine indentation depth. The method is applied to Vickers indentation of OFHC Cu and Ti–6Al–4V, and spherical indentation of 6061-T6 aluminum. An additional application is given with the aluminum alloy where a specially designed striker bar is used to partially unload the sample during loading, a technique that allows the contact area between the sample and the indenter to be estimated. In general, the method is applicable to a wide range of materials and indenter shapes and has the potential for loading times less than 5 μs.

Keywords High strain-rate · Indentation · Hardness · Kolsky bar · Split Hopkinson pressure bar

Introduction

Indentation is useful as a screening tool for materials, or to estimate mechanical properties when traditional mechanical testing methods are not practical or possible. Hardness values are typically determined from the maximum applied load and the size of the final impression made in the sample, for example Brinell [1], Knoop [2], and Vickers [3]. With instrumented indentation, however, the load and indentation depth are measured simultaneously, and considerably more

Emily Retzlaff is a member of SEM.

✉ D. T. Casem
  daniel.t.casem.civ@army.mil

  E. L. Retzlaff
  retzlaff@usna.edu

[1] DEVCOM Army Research Laboratory,
  Aberdeen Proving Ground, MD, USA

[2] Mechanical and Nuclear Engineering Department, United
  States Naval Academy, Annapolis, MD, USA

information about the material's behavior can be obtained [4–6].

Since material behavior is rate-dependent, there is interest in conducting indentation experiments at high loading rates. Complications that arise at high-rates include how to load the specimen, how to measure the rapidly changing load and indentation depth, and how inertia within the sample affects the hardness measurement. Recovery of the sample for post-mortem analysis can also be difficult. Several methods have been developed for high-rate indentation; some early methods include [7–10]. The present work is intended to supplement the Dynamic Indentation Hardness Tester (DIHT) developed by [11, 12], which is a modified Kolsky bar (Split Hopkinson Pressure Bar) to perform hardness tests with indentation times in the range of 100 to 500 μs. In this configuration, the indenter is mounted at the end of the input bar. The sample is mounted on a fixed base that incorporates a dynamic load cell. A striker impact drives the indenter tip into the sample and the indentation force is measured by the load cell. A momentum trap on a flanged input bar [13] is used to ensure the sample is only

loaded once. The indentation size is measured directly from the recovered sample, providing the information needed to determine a hardness value. The objective of the present work is to develop a miniature Kolsky bar method that can provide shorter loading times (as small as 5 μs) and offer an improved measurement of indentation depth measured simultaneously with the indentation force, along the lines of instrumented indentation methods.

Method

The experiment is shown in Fig. 1, and was originally described in [14]. The sample is fixed to the end of the input bar, and the input bar is impacted by a striker. If necessary, some type of pulse shaping can be used. The indenter is mounted/machined directly into the end of the output bar. It is assumed that these modifications do not affect its impedance substantially, and the output bar is treated as having a uniform impedance. A small gap can be left between the sample and the indenter tip to prevent premature loading. When the input pulse reaches the sample, the sample is driven towards the indenter tip. Upon contact, the force generated by the indenter transmits the output pulse into the output bar, and a reflection reflects back into the input bar.

The authors' current application is to supplement conventional (low-rate) hardness tests (Vickers, Knoop, etc.) on typical metals and ceramics. Forces are therefore expected to be low compared to conventional Kolsky bar testing. This requires low-impedance (small diameter) output bars to obtain sufficient force resolution. Conversely, typical samples will be relatively large, because of the need to keep the indentation site well away from the edges of the sample. These are paired with a similarly sized input bar, leading to the relative sizes suggested in the figure, i.e., a larger input bar and a smaller output bar. Depending on the exact sizes of the bars, they may be instrumented with either strain gages or interferometers [15, 16]. In the present work, strain gages are used on the input bar and a normal displacement

interferometer (NDI) is used on the free-end of the output bar. This is shown in the figure (NDI1), and the following equations assume this instrumentation.

Important displacement quantities are labelled in the figure. u_1 is the displacement of the end of the input bar, at the interface between the sample and the bar. u_2 is the displacement of the indenter tip. u_s is the displacement of the undeformed sample face, away from the indentation site, and u_f is the displacement of the free-end of the output bar. The corresponding velocities are v_1, v_2, v_s, and v_f.

The goal is to obtain an indentation-load vs. indentation-depth curve. To do so, the following analysis is performed. The force on the indenter tip (F_2) is obtained from the NDI1 measurement of u_f. Because NDI1 is located at a free-surface, the wave-separation is trivial and this can be done for all time, regardless of overlapping reflections, etc., using a modification of the standard analysis of the output pulse [15].

$$F_2(t) = \frac{A_o \rho_o c_o}{2} \left(v_f\left(t + \frac{L_o}{c_o} \right) - v_f\left(t - \frac{L_o}{c_o} \right) \right) \tag{1}$$

Here A_o, ρ_o, L_o, and c_o, are the cross-sectional area, density, length, and wave-speed of the output bar. The $\pm L_o/c_o$ terms in $v_f(t)$ account for backward and forward time-shifting by the time needed for the wave to travel the length of the output bar. If dispersion is significant, this time shift can be accomplished by a dispersion correction [17–20], identical to established methods, except that returning waves in the output bar must be corrected as well. These can be determined uniquely from the free-surface measurement [15].

Indentation depth, assuming an initial known gap of δ_{gap} between the sample and the indenter, can be found by the following equation, valid for times at which the sample and indenter tip are in contact.

$$\delta = u_s - u_2 - \delta_{gap} \tag{2}$$

u_2 is found from time integration of v_2, which is determined from an equation similar to Eq. (1) from the measured free-surface velocity [15]. Like Eq. (1), it is valid for all time.
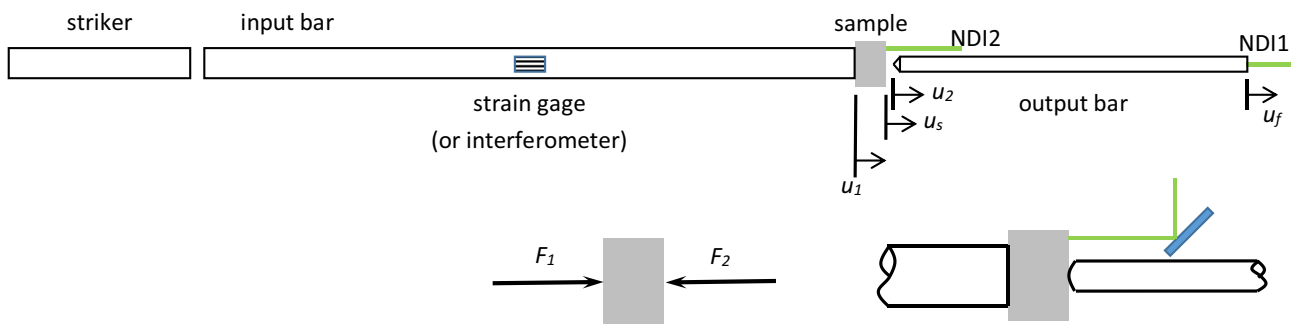

Fig. 1 A Kolsky bar for high-rate indentation

$$v_2(t) = \frac{1}{2}\left(v_f\left(t + \frac{L_o}{c_o}\right) + v_f\left(t - \frac{L_o}{c_o}\right)\right) \qquad (3)$$

The determination of u_s is less straightforward. If the sample is in equilibrium, the portion of the sample undisturbed by the localized indentation behaves largely as a rigid body, and one can assume

$$u_s = u_1 \qquad (4)$$

where u_1 and v_1 can be found from the standard analysis of strain pulses in the input bar.

$$v_1 = c_i\left(\epsilon_i - \epsilon_r\right) \qquad (5)$$

Here ϵ_i and ϵ_r are the input and reflected pulses (after correcting for dispersion and/or time shifting to the time they act at the sample interface), and c_i is the wave speed in the input bar. In many situations with small indentation depths, the assumption made in Eq. (4) is inadequate. It can be improved by matching the impedance of the sample to that of the input bar and adjusting the effective length of the bar to account for the time needed for the wave to traverse the sample, in which case Eq. (5) measures v_s directly. Sometimes this is not possible, as other considerations may dictate the sample size. Furthermore, the bond between the sample and bar, glue in most cases, could also introduce a small error. If the errors associated with these factors are unacceptable, u_s can be measured directly instead. This approach is taken in the spherical indentation applications given below, where an NDI is used directly on the sample as shown in Fig. 1, labelled NDI2.

The force between the sample and the input bar, F_1, can be found as well, although it is not needed for the current experiments and is unlikely to be as accurate as the F_2 measurement due to the relatively large impedance of the input bar for the forces that are generated at the indenter tip for samples of practical interest. In some situations it could be useful, and is easily determined with the standard equation.

$$F_1 = \left(\epsilon_i + \epsilon_r\right)E_iA_i \qquad (6)$$

If the indentation site must be preserved for post-mortem measurements, it is important to ensure that the sample is only loaded a single time. As with any Kolsky bar, reverberations of the reflected pulse in the input bar may cause the sample to reload, and special precautions must be taken to prevent this. As mentioned above, the DIHT uses a flanged input bar with a momentum trap, essentially a modification of the method used by [13]. Another possibility is to use mechanical stops around the specimen ("stop rings") to directly limit sample deformation, and a similar technique could be devised for indentation.

Still another technique is to choose test parameters such that the wave mechanics in the bars avoid sample reloading "naturally," in a generalization of the method used by da Silva

and Ramesh [21]. The sample is initially loaded due to the actions of the input, reflected, and output pulses. This is the loading that is used to determine the sample's mechanical response. The reflected pulse will then reverberate in the input bar, periodically driving the end of the input bar towards the sample, separated by the time needed for the pulse to travel twice the length of the bar. This will in general cause the sample to re-load. However, the output pulse will also reverberate in the output bar. These reverberations drive the output bar away from the input bar, again in periodic increments separated by the time needed for the wave to travel twice the length of the output bar. If the motion of the output bar exceeds that of the input bar, the sample will not re-load, and the bars can eventually be arrested in a variety of ways that allow soft recovery of the sample. The displacement associated with these reverberations are proportional to the time integral of the reflected and output pulses; a large reflection makes recovery less likely, while a large output pulse makes recovery more likely. Decreasing output bar impedance (diameter) and length therefore increases the likelihood of recovery. This makes this approach ideal with the present technique, since, as explained above, a relatively short, small diameter, output bar will often be needed to meet other testing requirements.

Natural recovery, however, can complicate the design of the experiment, since the post-test wave mechanics in the bars must be considered in the selection of the other experimental parameters—geometry and material of the bars and striker, impact speed, and the possible use of a pulse shaper. This is not always trivial. Furthermore, since output bars with integrated indenters generally need to be custom-made, there is the additional incentive to design the components such that the range of application of a given indenter (different sample materials, maximum loads, indentation rates) is as large as possible. For these reasons, the method described in [22] is recommended. The method in [22] allows the experimental results to be approximated in advance so that the effect of changing one aspect of the experiment (striker speed, output bar length, etc.) can be determined. Most research groups perform some level of similar analysis prior to testing; [22] does this in a general way. This allows the experiment to be designed logically and precisely. To use the method, the approximate behavior of the sample must be known in advance. Since this is almost always the case (for example, from the results of low-rate indentation experiments or a few preliminary high-rate experiments), this provides a useful tool to design the experiment to obtain the desired sample loading. In [22], the wave propagation in each bar is described by the D'Alembert solution. This full treatment is useful because it accounts for returning waves and superimposed waves, which are usually avoided in most Kolsky bar descriptions. In the example at the end of the next section, this method is also used in conjunction with Bacon's method [23] to iteratively design a striker geometry

to partially unload and reload a sample. This is described in detail in [22]. A simplified version of this method, with application to the natural recovery, is given in the appendix.

Applications of the high-rate indentation method are given in the following sections and include (i) Vickers hardness of OFHC Cu and Ti–6Al–4V and (ii) spherical indentation of 6061-T6 aluminum.

Application—Vickers Indentation of OFHC Copper and Ti–6Al–4V.

High-rate Vickers indentation is a simpler application because there is no need to measure the indentation depth, δ, and NDI2 can be omitted. The final indentation size is obtained by averaging the two diagonal lengths measured with a microscope after the load is removed (d_{diag}). A Vickers hardness value, HV, can then be obtained from the following equation.

$$HV = \frac{1.8544P}{d_{diag}^2} \tag{7}$$

P is the applied load and the constant is dictated by the geometry of the indenter. In the conventional Vickers hardness test (low-rate), a known load is applied slowly in a controlled manner and removed after being held steady for 10–15 s. In the high-rate test, P is the peak load applied at the indenter tip, no matter how briefly. For these experiments, high and low-rate Vickers hardness tests were conducted on OFHC Cu and Ti–6Al–4V. The low-rate tests were conducted with a Sun-Tech Corporation CM-400AT hardness tester with loads of 0.30, 0.50, and 1.00 kg-f (2.94 N, 4.90 N, 9.81 N), and hold-times of 15 s.

For the high-rate tests, a Vickers diamond indenter was mounted by Gilmore Diamond Tools, Inc., directly into a small recess machined in the end of a 1.59 mm diameter tool steel output bar. The total length (tip of indenter to the end of bar) is 49 mm. An image of the indenter is shown in Fig. 2. It is assumed this has a negligible effect on the bar's impedance and the bar is treated as having uniform properties like a standard output bar. The other end of the output bar is polished to a specular finish for NDI1. The input bar was made from aluminum 7075-T6 and had a diameter of 4.76 mm and a length of 743 mm. The input pulse and reflection are measured with straingages mounted 193 mm from the sample end. A 51 mm long, 3.18 mm diameter 7075-T6 aluminum striker is used to load the sample, with a small amount of vacuum grease as a pulse shaper, just enough to increase the rise-time of the input pulse and reduce dispersion. This choice of geometry, especially the unusually long input bar and short output bar, was made so that natural recovery would occur over a wide range of testing using the analysis of [22]. A
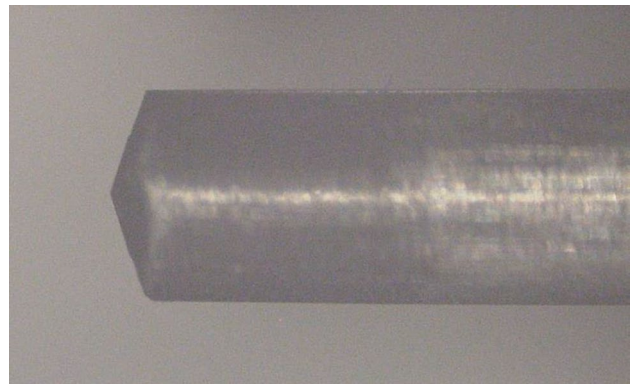

Fig. 2 A 1.59 mm diameter steel output bar with a Vickers diamond indenter

simpler version of this analysis as applied to the experiments discussed in this section is given in the Appendix.

The samples were cylindrical with lengths and diameters of 3.18 mm. The indentation faces were lapped flat and polished to a 0.5 μm finish. They were glued to the end of the input bar with cyanoacrylate adhesive. The indenter is positioned with a micrometer head mounted in a custom-made fixture while viewing under a stereoscope. Using this method, small gaps (< 10 μm) could be reliably left between the sample and indenter tip prior to each experiment to prevent premature loading of the sample.

It is convenient to make multiple measurements on a single sample. This was accomplished by raising the axis of the output bar relative to the input bar by 0.72 mm. In this way, the indentations are not located at the center of the sample, but 0.72 mm above. After each experiment, the input bar (with sample attached) can be rotated (~ 45°) so that the next indentation is at a new location. In this way, multiple indentations can be made in a ring around the sample face while maintaining appropriate spacing between indentations and from the sample boundaries. This results in a non-centric loading on the input bar, although any error introduced by this is unimportant in the analysis. After testing, the sample is removed to a microscope for measurement of diagonal lengths. An example of the measured load, using Eq. 1, is shown in Fig. 3. This is an experiment on Cu, with a peak load of 11.1 N. The entire loading cycle, including the unloading, is about 25 μs. All the high-rate Vickers experiments, regardless of peak load, have similar loading times.

The results of the Vickers hardness experiments are shown in Figs. 4 and 5. Figure 4 shows load plotted vs. the square of the averaged diagonal lengths, following Koeppel and Subhash [12]. Linear fits are also given, the slopes of which give a measure of the low and high-rate Vickers hardness for each material when multiplied by the geometric factor in Eq. (7).

Alternatively, hardness values for each individual experiment can be calculated. This is done in Fig. 5, along with linear fits to each group of data. One disadvantage of the

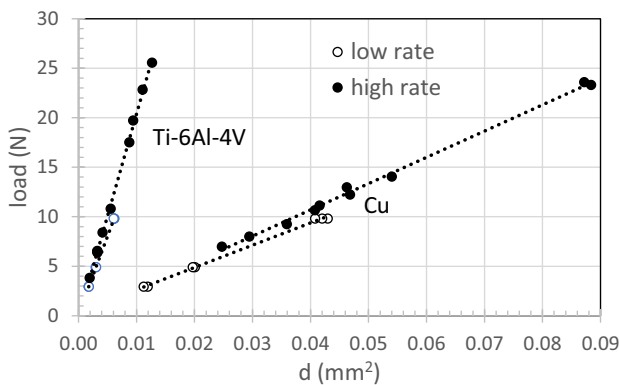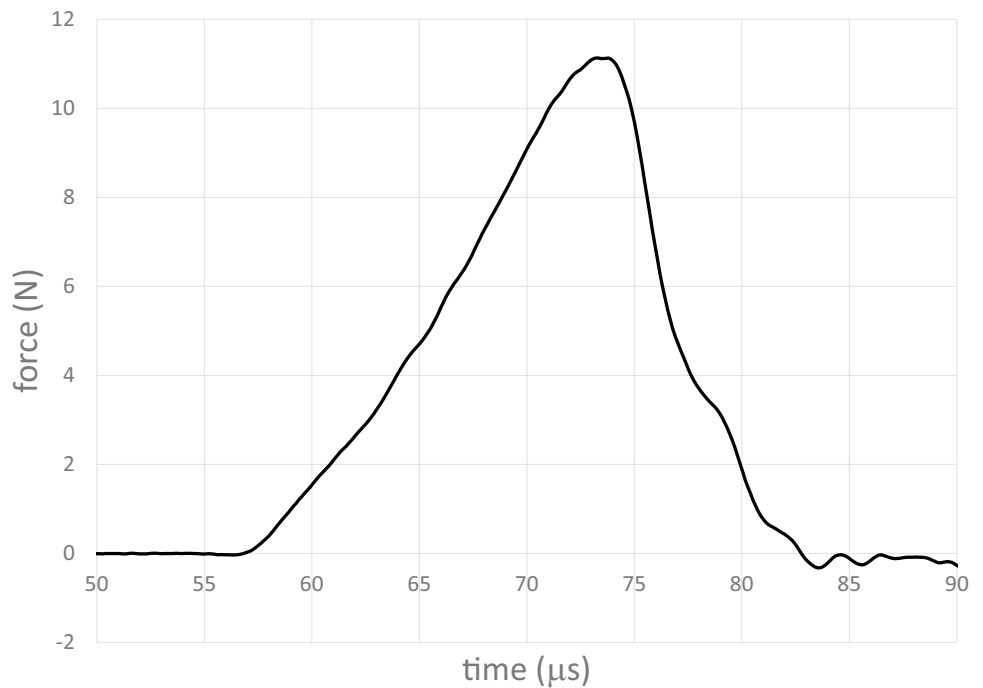**Fig. 3** Load vs time for a high-rate indention experiment on OFHC copper

Fig. 4 Indentation load vs. the square of the average diagonal length for low and high-rate Vickers indentation of Ti–6Al–4V and Cu. The dotted lines are linear fits, which provide a measure of the hardness and show the rate effect
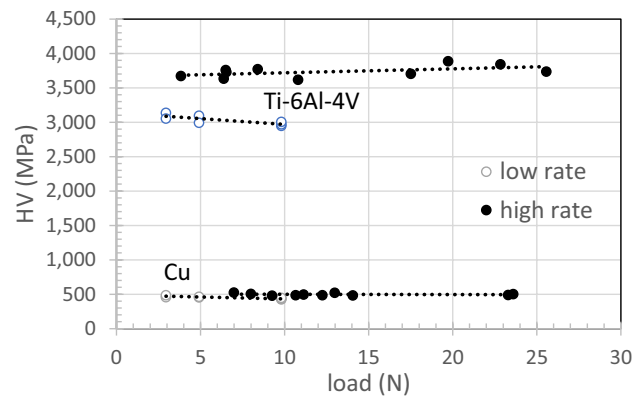

Fig. 5 Vickers hardness values over a range of loads at both high and low loading rates

high-rate experiment is that it is difficult to reliably apply a precise load to the sample, which is not an issue with the low-rate experiments. To compare the high-rate values to the low-rate values at some particular load, some method for interpolation is therefore needed. In this case, the linear fits are used.

Table 1 shows hardness values for both materials at low and high rates using the slope method from Fig. 4 and the interpolation method from Fig. 5, the latter for an applied load of 9.81 N. For both materials, HV clearly increases with rate. Koeppel and Subhash [12] made similar comparisons (slope method) for numerous materials, including OFHC

Table 1 Summary of Vickers hardness

Material	Rate	HV at 9.81 N (MPa)	HV from linear fit (MPa)
OFHC Cu	Low	434.1	417.1
OFHC Cu	High	498.0	491.6
Ti–6Al–4 V	Low	2974	2919
Ti–6Al–4 V	High	3718	3818

The HV values at 9.81 N are from Fig. 5 and the values in the right-most column are from the linear fits in Fig. 4

copper and Ti–6Al–4V, so the results can be compared. They found increases in high-rate hardness over the low-rate values for OFHC Cu and Ti–6Al–4V of 17.8% and 21.0%, respectively. Our results (slope method) show increases of 15.0% and 25.3%, which is consistent with their previous work.

Koeppel and Subhash also used their low and high-rate HV data to generate a relationship between flow stress Y (true stress at 8% true strain) and HV. The found the following correlations, based on data from 19 metals and alloys.

$$Y_{low} = HV_{low}/3.025 \qquad (8)$$

$$Y_{high} = HV_{high}/2.875 \qquad (9)$$

This can be applied to the specific Ti–6Al–4V here, which has been characterized mechanically over a wide range of strain-rates [24, 25]. It is difficult to estimate strain-rates for indentation, but following [12] we take the strain-rate of our low-rate experiments to be 0.001/s and the strain-rate of our high-rate experiments to be 10,000/s. In [12] they assumed a strain-rate for their high-rate experiments of 2000/s; our experiments are about 1/5 the loading duration so it is reasonable to assume the higher strain-rate. We do not expect a large change in behavior over this range anyway because [24, 25] found no enhanced rate effect for this material; the flow stress was linear with the logarithm of strain rate over the entire strain-rate range studied (0.001/s to 700,000/s). The measured flow stress and that predicted from the hardness values and Eqs. (8) and (9) are given in Table 2. The predicted values are 8.5% and 5.6% lower than the measured values, again in good agreement with [12] considering the scatter in the data and other experimental uncertainties.

Application—Spherical Indentation of 6061-T6 Aluminum

High-rate spherical indentation results for 6061-T6 aluminum are now presented. The objective here is not to determine a hardness measurement, but to obtain the full load vs indentation depth curve, so that material properties can be estimated. This involves an inverse method with finite elements. Some details of these efforts can be found in [26–28], and here the focus is on describing the

Table 2 Measured flow stress compared to that predicted from the hardness values for Ti–6Al–4V

Rate (1/s)	HV at 9.81 N (MPa)	Measured flow stress (MPa)	Predicted flow stress (MPa)	Error (%)
0.001	2974	1075	983	− 8.5
10,000	3718	1370	1293	− 5.6

experimental technique. The output bar was 1.59 mm diameter tool steel (Rockwell C60) with a 102 mm length. The indenter end was machined (Gilmore Diamond Tools, Inc.) to a slight curvature with a 6.35 mm radius. This is depicted in the lower right schematic in Fig. 1, although the curvature is greatly exaggerated. This is a minor modification of the usual flat-end geometry, and the output bar is treated as having a uniform impedance. NDI1 measures u_f and v_f.

Samples are cylindrical, with length of 3.6 mm and diameter of 4.8 mm. The indentation faces are lapped flat and polished to a 0.5 μm finish. The sample is glued to the end of the input bar with cyanoacrylate. The input bar is 458 mm long, 3.18 mm diameter, and made from 7075-T6 aluminum. Ideally, the sample diameter would match the input bar, resulting in an almost perfect impedance match. However, an oversized sample was used here to provide more space to instrument the sample face with NDI2, which is focused between 0.4 and 0.6 mm from the sample edge. The details of the NDI implementation are given in [25]. The use of NDI2 is somewhat difficult because of the presence of the output bar and its bushings. Thus a mirror is used to direct the beam to the sample face, as shown in Fig. 1, inside the focusing lens shown in reference [25]. The NDI is otherwise identical to the interferometer described in that reference.

Typical indentations are 0.7 mm in diameter, so the NDI2 measurement is made approximately 1.5 mm from the edge of the indentation. It is assumed that the motion of the measurement point is not affected by the indentation, and that this is an accurate measurement of u_s. No lubrication is used between the indenter and the sample. There is a risk of local sample heating when instrumenting with a laser directly. This was minimized by exposing the sample to the laser only briefly (< 2 s) prior to testing. Both NDIs operate at 532 nm wavelength. The input bar is instrumented with strain gages (two gages mounted diametrically opposed to cancel components due to bending) at the midpoint of its length.

The striker is similar to the input bar but only 25 mm long. A small amount of solder is used as a pulse shaper, held in place with vacuum grease. As before, small gaps are left between the indenter tip and the sample prior to testing (< 10 μm). Although these gaps were not measured, the time the sample and indenter tip make contact can be determined from the F_2 measurement, i.e., when the force first begins to rise. Identification of the initial contact, or "zero point", is an issue in low-rate indentation experiments, and methods have been developed to do this with more precision. In [29] for example, fits are made to the initial portion of the force vs. indentation depth curve, which is assumed elastic, to the Hertzian contact solution. This was not done here mainly because it is unknown how much of the initial loading is elastic, so the zero-point is instead estimated from the initial rise in indentation force.

Data from an example experiment is shown in Fig. 6. The input pulse and reflection are measured by the strain gages, and the input pulse shows the effect of the pulse shaper. The motion of the sample face is measured directly by NDI2, giving v_s. The velocity of the free-end of the output bar (NDI1) starts to rise at 122 μs due to the arrival of the stress wave caused by contact with the sample. There are two humps in this trace, the second due to the reflection of the "output pulse" from the indenter end of the bar reaching the free end. This trace is used in Eqs. (1) and (3) to determine F_2 and v_2. Again, there is no need to separate this reflection from the output pulse as this is accounted for in the calculations, and these measurements are valid for as long as there is recorded data.

Figure 7 shows v_s repeated from Fig. 6 along with the calculated velocity of the indenter tip, v_2. The difference between the two gives the rate of indentation depth, dδ/dt. The force on the indenter tip, F_2, is shown on the secondary axis. Several times of interest are marked by vertical dashed lines. The initial contact of the indenter and sample occurs at 102 μs, when the force begins to rise. The indentation rate stays positive until 128 μs, when a peak force is achieved, and the sample begins to unload (dδ/dt is negative). The rate is not constant but could be made so with appropriate pulse shaping. The unloading is complete at 148 μs, when the force returns to zero. The motion of the indenter tip after this time is due to waves reverberating in the output bar as it travels away from the sample. This later motion essentially repeats for all time,

until mechanical stops (not shown) arrest the motions of the bars. This ensures the sample is not reloaded.

Integrating the indentation rate gives the indentation depth. Force vs. indentation depth for this experiment is shown in Fig. 8, labelled 1. Four repeated experiments are also shown (labelled 2–5).

Figure 9 shows load vs indentation depth for three additional experiments on 6061-T6 aluminum. These tests used a tungsten carbide (WC) indenter/output bar. The output bar has a 1.59 mm diameter and a 38 mm length. A sharper spherical indenter shape is used in this case with R = 3.18 mm (again provided by Gilmore Diamond, Inc.). As before, this is a minimal modification of the normally flat output bar so the small change in impedance at the indenter end is ignored. The loading times are shorter in these cases (~ 13 μs) due to the shorter output bar length and higher wave speed in the WC. By varying the striker speed, a range of indentation depths were obtained, notably larger than in the experiments discussed above. All three samples were naturally recovered after a single loading/unloading.

After recovery, these larger indentations were measured with a Keyence VK-X200 confocal microscope, allowing a direct measurement of the final indentation depth. This can be compared to the final indentation depths from Fig. 9, after the elastic recovery when the indentation load returns to zero. The error associated with the confocal microscope is estimated at ± 0.3 μm, mainly due to the subjective nature of identifying the initial undeformed surface that is not perfectly flat. The final depths are given in Table 3.

Fig. 6 Data collected from an experiment on aluminum 6061-T6. ε_i, ε_r, v_s, and v_f are all shown
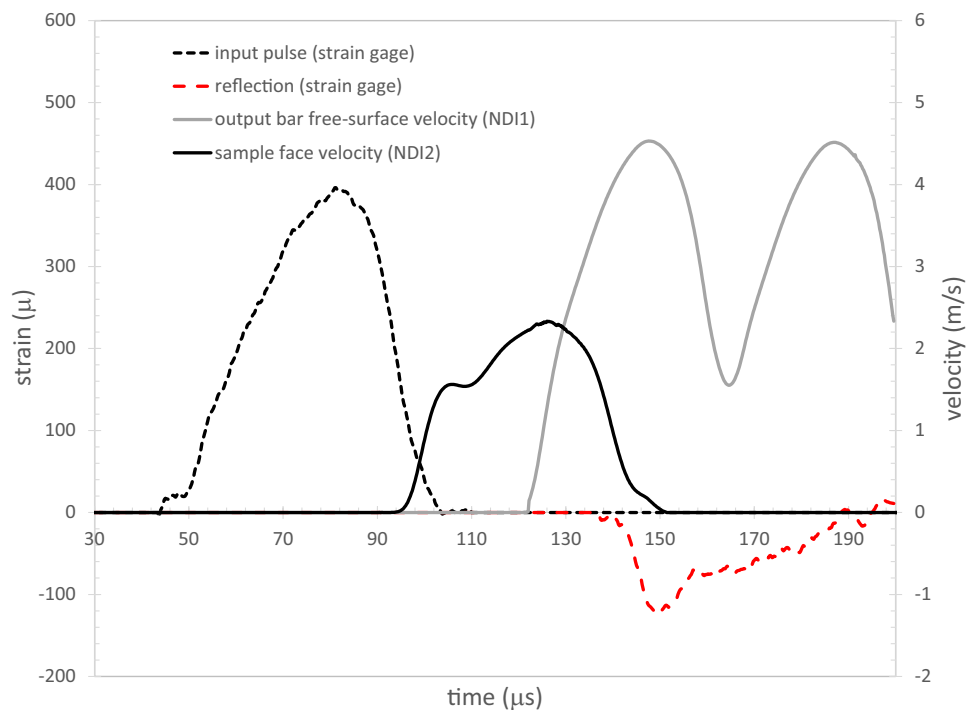
Fig. 7 Velocities of the sample face and the indenter tip (black solid and dashed); the difference is the rate of indentation into the sample (grey). The force on the indenter tip is also shown (red). The dot-dashed vertical lines denote the initial contact (closure of the initial gap between the sample and indenter tip), the peak load when the sample begins to unload, and the time when the sample and indenter tip separate (Color figure online)
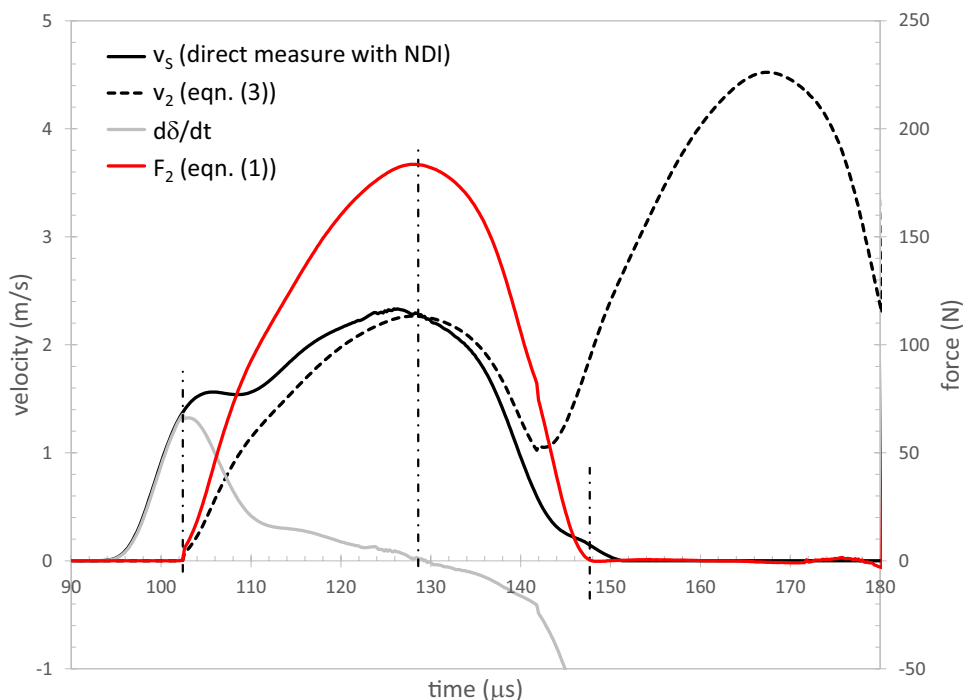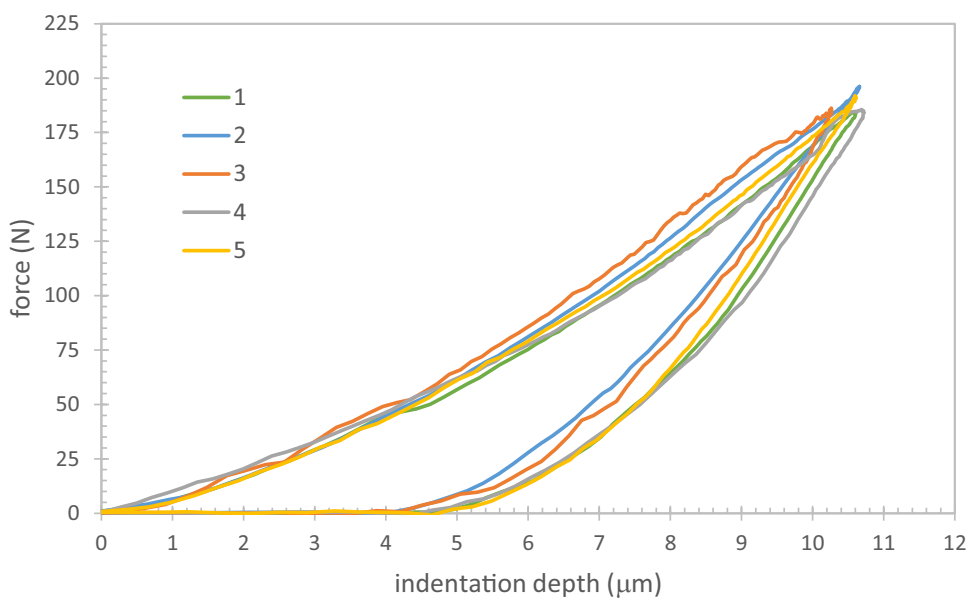

Fig. 8 Five repeated high-rate indentations into 6061-T6 (R = 6.35 mm steel indenter). The loading times are between 20 and 30 μs

In all three cases, the final depths are within the estimated error bounds.

Another way to judge the accuracy of the indentation depth measurement is to compare the reduced modulus of the contact system determined from elastic properties (sample, E, v, and indenter, E_i, v_i) to that estimated from the initial portion of the unloading curves in Fig. 9, dP/dδ. From [30], the effective modulus is as follows.

$$\frac{1}{E_r} = \frac{(1 - v^2)}{E} + \frac{(1 - v_i^2)}{E_i} \tag{10}$$

As calculated from the unloading stiffness,

$$E_r^* = \frac{dP/d\delta}{D_f} \tag{11}$$

Fig. 9 Larger indentations into 6061-T6 aluminum using a sharper (R = 3.18 mm) WC indenter bar. Larger loads and indentation depths were achieved in these cases
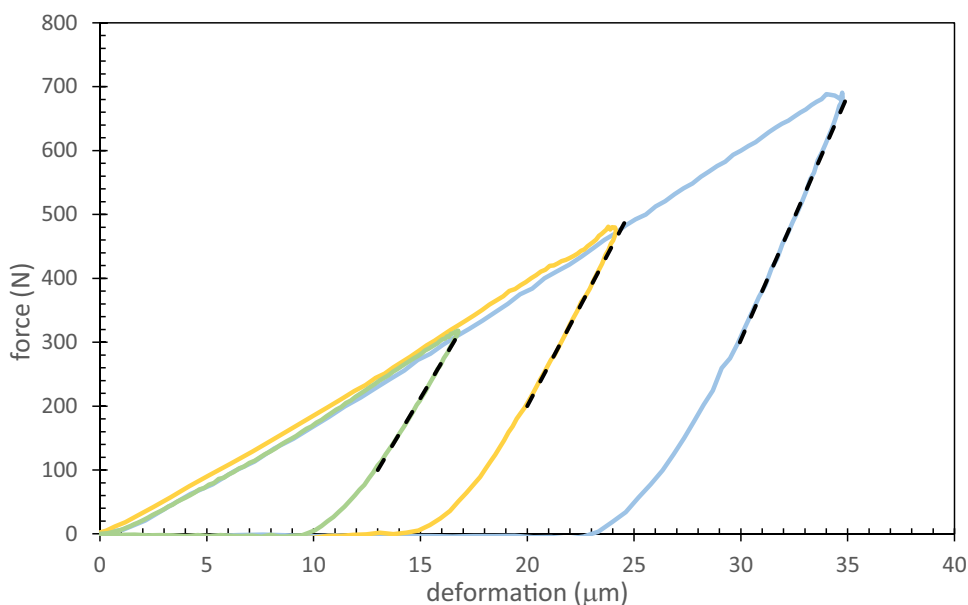

Table 3 Summary of the final indentation depths made by the R = 3.18 mm WC indenter: a comparison between that measured with the Kolsky bar analysis (the final indentation depth, at zero force in Fig. 9) and confocal microscope measurements on the recovered samples

Final indent depth			Reduced modulus			
Kolsky bar (μm)	Microscope (μm)	Error (%)	dP/dδ (N/μm)	D_f (μm)	E_r^* (GPa)	Error (%)
9.9	10.1	− 2.0	56	706	79	11.5
14.5	14.7	− 1.4	63	843	75	5.0
23.0	22.8	0.9	77	986	78	9.8

The reduced modulus calculated from Eq. (11) is also given, using the slopes shown in Fig. 9

where D_f is the diameter of the final impression measured post-test with a microscope, and the unloading stiffness is the slope of the initial portions of the unloading curves in Fig. 9. For this system, (E_i = 682.5 GPa, ν_i = 0.25, E = 69.2 GPa, ν = 0.35) the reduced modulus is E_r = 71.2 GPa. The reduced moduli calculated from Eq. (11), using the slopes depicted in Fig. 9, are given in the table. The error between these values and that determined from Eq. (10) are also given. In each case, the values predicted by the unloading stiffnesses are higher than that predicted from the elastic properties, by between 5 and 11.5%.

Application—A Tapered Striker to Partially Unload the Sample

The next example shows a method to partially unload and reload a sample during indentation. This is useful with spherical indentation because it allows the contact area between the indenter and the sample to be estimated, improving the accuracy of mechanical data inferred from indentation experiments. With commercial indentation equipment, this can be achieved via the Continuous Stiffness Measurement (CSM) feature [4]. For equipment that lacks CSM, partial unloadings are used instead. In [5], this process for spherical indentation is described. Assuming the unloading path is elastic, the contact radius can be estimated by comparing the measured unloading/re-loading path to the Hertzian contact theory. The challenge with the high-rate experiment is generating the unloading. Note a full unloading is not desired, since the re-loading on a sample that has separated from the indenter may not be perfectly aligned with the initial indentation. The approach taken here is to pulse shape so that the input pulse decreases in magnitude temporarily so that the sample can unload. This is done by using a striker bar whose impedance varies in such a way to create a suitable input pulse; i.e., a striker that is considerably reduced in area in the middle than at the ends. Such a
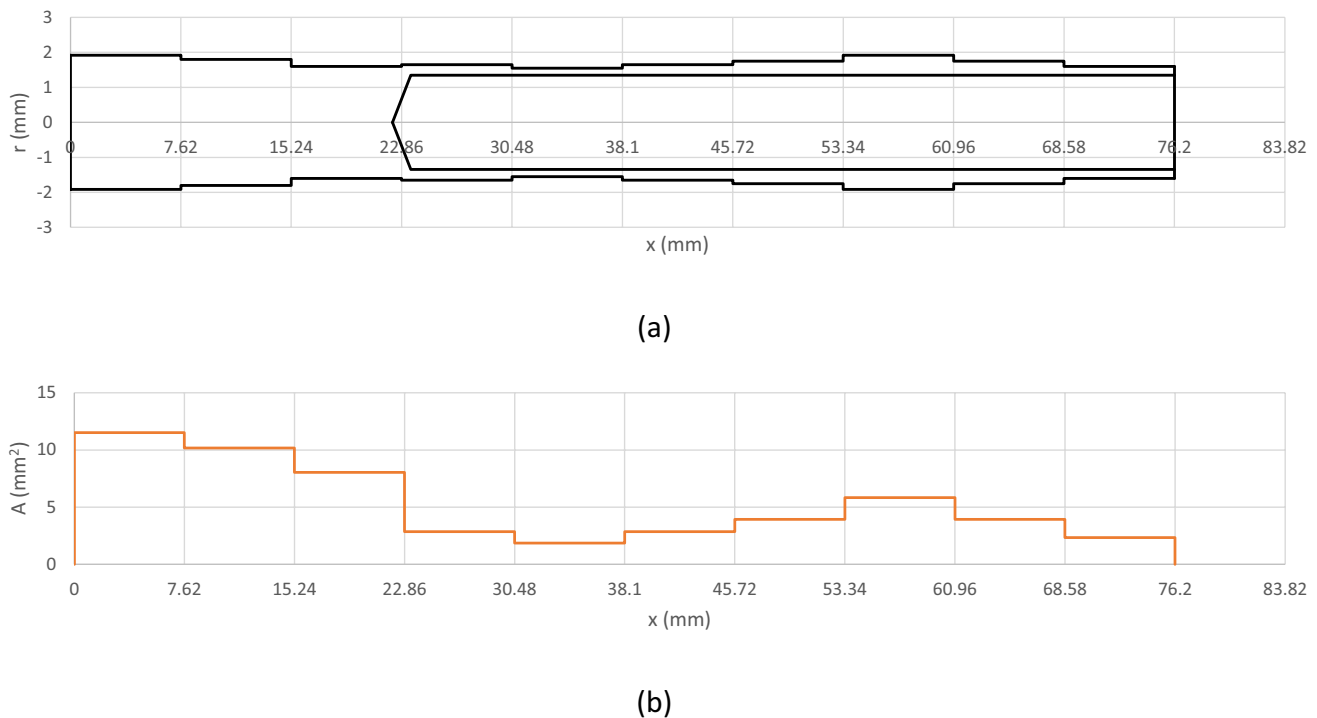
(a)

(b)

Fig. 10 a A graded impedance projectile used to create a partial unloading during indentation. The "negative radius" is plotted to help visualize the shape. Note the horizontal and vertical scales differ. The hollow end on the right side impacts the input bar. **b** The variation of cross-sectional area

striker bar was designed for the aluminum experiments using the iterative method by Bacon [23]; see [22] for more detail.

The final projectile shape is shown in Fig. 10a, and the variation of area in Fig. 10b. The impact end is to the right, and the total length is 76.2 mm. It was made from 7075-T6 aluminum. The area was reduced by both removing material from the outer surface and by hollowing one end. This simplifies machining, helps avoid buckling, and also leaves a convenient shape for launching from the gun barrel (the outer diameter matches the bore of the barrel at two locations so no sabot is needed). Additional pulse shaping was achieved by adding a single layer of cellophane tape to the impact-end of the input bar. This was done mainly to increase the rise-time. An example of the resulting input pulse is shown in Fig. 11. The specimen is 6061-T6 aluminum and the indenter is 1.59 mm diameter steel with a 6.35 mm radius indenter surface. The velocities measured by the two NDIs, v_s and v_f, are also shown. The temporary decrease in the input pulse magnitude is clear. v_s is repeated in Fig. 12 along with F_2, v_2, and $d\delta/dt$. The first dashed vertical line marks the initial contact, when the gap between the indenter and sample closes and the load starts to increase. The next two dashed lines mark the start and end of the unloading, when $d\delta/dt$ is negative.

The unloading occurs over about 8.5 μs. The sample then reloads and unloads completely. Force is plotted with indentation depth in Fig. 13. The unloading and reloading shown is assumed elastic. The re-loading path matches the unloading path closely, although some disagreement is seen upon closer inspection of the data shown in the inset.

Discussion and Conclusion

An indentation method capable of measuring load vs. indentation depth at high-rates has been presented. The examples given have loading times in the range of 10 to 50 μs, about a factor of 5 faster than other Kolsky bar methods. Even at these rates, the time resolution is good. This is due to the use of small diameter output bars. Reducing bar diameter decreases the bar's rise-time, and further miniaturization could permit shorter duration tests. This is the fundamental limitation of the method, i.e., how small can bars be made that incorporate suitable indenters. Changing bar diameter of course affects other aspects of the experiment—the maximum load that can be achieved, the sensitivity of the force and displacement measurements, the requirements of pulse shaping—in a way that is not entirely straightforward. For

Fig. 11 Measured data from an experiment using a graded-area projectile to allow the sample to temporarily and partially unload. ε_i, ε_r, v_s, and v_f are all shown
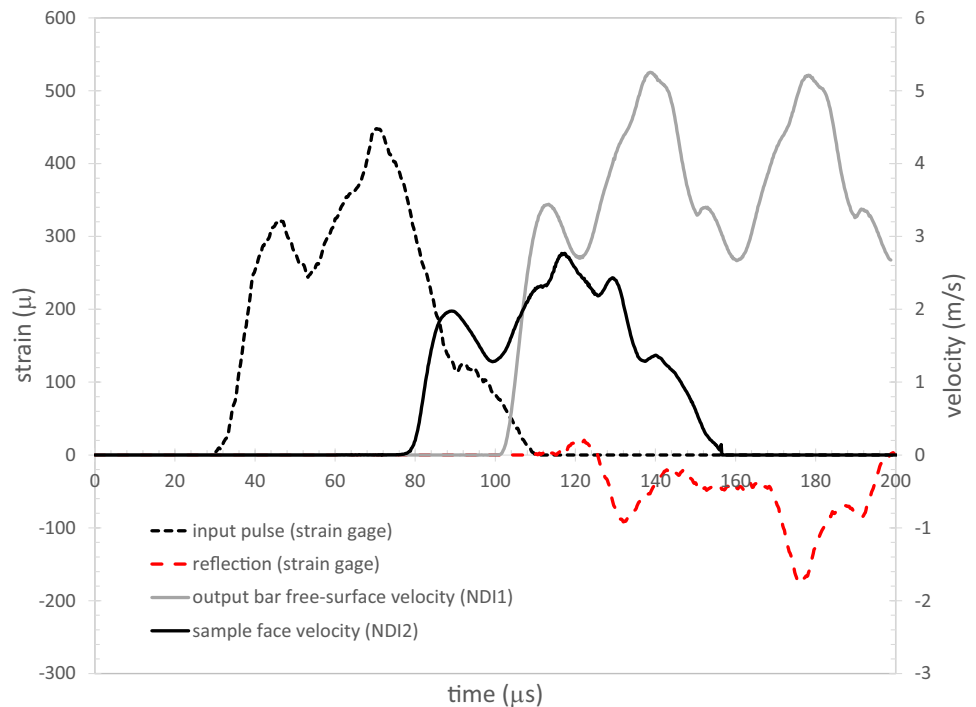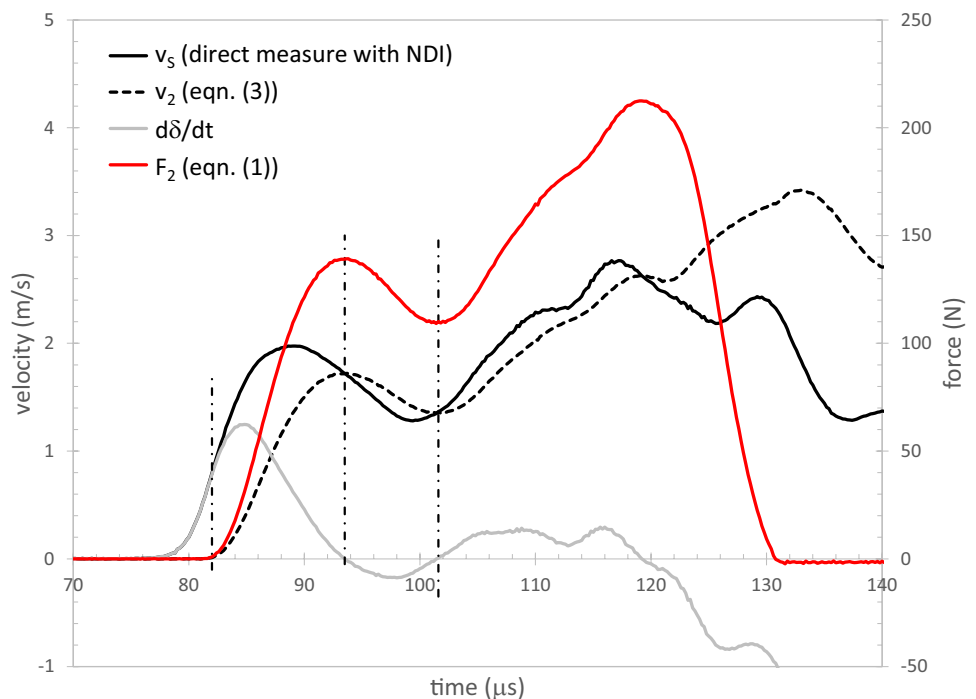
Fig. 12 Relevant velocities and indentation force for the partial unloading experiment. Note the brief negative indentation rate (grey) between 93.5 and 102 μs; this is when the unloading occurs (Color figure online)

this reason, the test-design methods described in the appendix or [22] are recommended. The interferometer measurements used here are well-suited to this application. Other instrumentations, for example Photon Doppler Velocimetry [31], could be used as well.

Since the main feature of the method is the use of a small diameter output bar with an embedded indenter, the use of the input bar to drive the sample into the indenter is less relevant. It seems reasonable that some modified form of this method could be used with more conventional indentation equipment to increase the indention rates that can be obtained. The output bars used here were free at one end; although analysis methods exist for bars in which this is not the case. Thus this approach that essentially treats

Fig. 13 A high-rate indentation experiment on 6061-T6 aluminum in which the sample is partially unloaded and reloaded. The time difference between circular markers in the inset is 0.2 μs; the duration of the entire experiment is about 48 μs
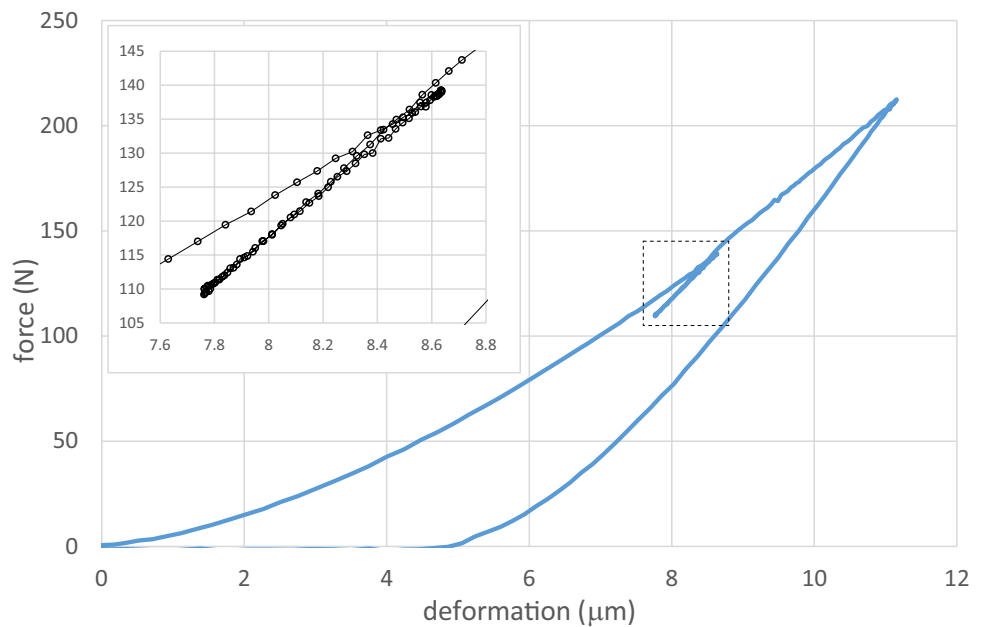
the indenter-bar as an instrumented wave guide can potentially be applied to a range of indentation configurations.

The use of high-rate Vickers indentation to estimate rate sensitivity of the flow strength of metals was shown by [12], and the current work supports this application. With the ability to reach shorter loading times, and potentially higher strain-rates, it seems reasonable that experiments could be performed at rates where phonon drag effects are significant. This can provide a simple method to study this phenomenon, avoiding the obstacles that occur in other experimental methods [32] such as direct mechanical testing with miniature Kolsky bars [25].

The error associated with this technique needs further consideration, especially concerning indentation depth. The good agreement between final indentation depths as measured by the confocal microscope and from the load-indentation depth curves (Table 3) is encouraging. However, the consistent over-estimate of unloading modulus when compared to calculated values (Table 3) may indicate some systematic error. The interferometers as implemented here are accurate to within a fraction of an interference fringe, likely on the order of a few tens of nanometers. This implies very accurate measurements of u_s and u_f by Kolsky bar standards, which are typically instrumented with conventional strain gages with an accuracy on the order of 1%. Some additional error will exist if the surface at the measurement location is not perfectly normal to the load direction or if the interferometer is not perfectly normal to the sample face. Alignments to within 1 degree are typical, which implies these errors are less than 0.1%. Larger errors arise due to uncertainties in the parameters needed in Eqs. 1 and 2 to calculate u_2 and F_2, and due to the assumption that the wave

propagation obeys the one-dimensional theory. Although there is nothing unusual about these errors, indentation measurements are often used to infer elastic properties, so slight errors can have a significant effect. Thus further quantification of the error of the displacement measurement may be needed if this is an objective. There seems to be no issue with the accuracy of the force measurement, and if indentation size is measured from the recovered sample as in the case of Vickers hardness then none of this is an issue.

Finally, equilibrium is an interesting issue with dynamic indentation. While the samples can be quite large, the deformation is localized to a small volume near the indenter tip, so the effective sample size can be small. This implies equilibrium can be achieved rapidly. How elastic and plastic waves in the sample affect the measured hardness values is an additional area for future work.

Appendix

This appendix describes an approximate method to ascertain if a sample will be re-loaded after the initial loading cycle, i.e., if the sample will be naturally recovered. This can be done prior to actual testing if an estimate of the expected sample behavior is known. If the analysis shows that the sample will be re-loaded, test parameters (striker speed or length, and/or bar lengths, material, or geometry) can usually be adjusted so that re-loading can be avoided. If this is not possible, recovery can then be achieved using other methods (input bar momentum traps or mechanical stops to limit the indentation depth). The method is demonstrated

for Vickers indentation but could easily be extended to other loadings. Several simplifying assumptions are made, and for situations where these assumptions are inadequate, or for non-indentation applications, the more detailed method described in [22] is recommended.

During indentation, the sample face is driven into the indenter tip. The difference between the motions of the sample face and the indenter tip is the indentation depth, provided the sample is in contact with the indenter. The indentation depth is therefore calculated from the motion of the ends of the bars. After the initial loading, the sample unloads, and the reflected pulse and output pulse propagate into the input and output bars, respectively. The later reverberations of the input pulse in the input bar will typically drive the sample into the indenter tip, potentially reloading the sample. However, the reverberations of the output pulse in the output bar will cause the indenter tip to move away from the sample, reducing the likelihood of re-loading. If the motion of the latter exceeds the motion of the former, natural recovery is assured. The motion of the sample face is related to the time integral of the reflection and the motion of the indenter tip is related to the time integral of the output pulse. Thus, the method depends on predicting the output and reflected pulses. This can be done if an estimate of the sample behavior is known in advance, which is almost always the case. It is essentially the reverse of a typical Kolsky bar analysis, where the measured output and reflected pulses are used to determine sample response. In the reverse, the sample response is used to determine the output and reflected pulses, under the assumption that the input pulse is a known quantity.

Begin by assuming the sample behavior in the form of a force vs. indentation depth response. This can be adequately approximated from conventional hardness measurements, since it is not expected that the high-rate behavior will differ excessively from that observed at low rates. Alternatively, it can be measured in a preliminary high-rate experiment. Ignore any indentation size effect and use the equation for Vickers hardness to determine load as a function of indentation depth from a known low-rate HV value. The standard equation for Vickers Hardness is given in Eq. (7). Assume this equation holds throughout the deformation, not just at the final state. Also ignore elastic unloading. The indentation depth for this indenter geometry is 1/7 of the diagonal length, thus a relation between P and δ can be found.

$$P = 26.43HV\delta^2 = M\delta^2 \tag{12}$$

The constant $M = 26.43HV$ is introduced for convenience. Assume the sample is in equilibrium, thus

$$P = F_1 = F_2 \tag{13}$$

Equation 6 is next used to relate the reflected pulse to the sample response.

$$\epsilon_r = \frac{P}{E_i A_i} - \epsilon_i = \frac{M\delta^2}{E_i A_i} - \epsilon_i \tag{14}$$

Here ϵ_i is the known input pulse. It is typically a rectangular pulse but can be more complicated if pulse shaping is used. Note ϵ_i, ϵ_r and ϵ_0 are assumed translated in time to the time they act simultaneously at the sample, not when they are measured at a more-or-less arbitrary gage location. Similarly, the output pulse can be related to P and δ.

$$\epsilon_o = \frac{F_2}{E_o A_o} = \frac{P}{E_o A_o} = \frac{M\delta^2}{E_o A_o} \tag{15}$$

Assume there is no initial gap between the sample and indenter. Equation (2) can then be used to relate the rate of indentation to the velocities of the ends of the bars.

$$\dot{\delta} = v_1 - v_2 \tag{16}$$

v_1 is related to the reflection by Eq. 5, and a similar equation can be written that relates the output pulse to v_2.

$$v_2 = \epsilon_o c_o \tag{17}$$

Equation (16) then becomes

$$\dot{\delta} = c_i(\epsilon_i - \epsilon_r) - \epsilon_o c_o \tag{18}$$

Substituting Eqs. (14) and (15) gives

$$\dot{\delta} = c_i\left(2\epsilon_i - \frac{M\delta^2}{E_i A_i}\right) - \frac{M\delta^2}{E_o A_o}c_o \tag{19}$$

Because ϵ_i is an arbitrary function, depending on the pulse shaping, this equation is best solved numerically. Once $\dot{\delta}$ is known, δ can be determined from time integration. Then Eqs. (12), (14), and (15) can be used to determine the load history of the sample (including the peak load), the reflected pulse, and the output pulse.

At this point, the average velocity of the sample face and indenter tip can be estimated, assuming no further contact between the two. If the latter is greater than the former, natural recovery should occur. If not, the assumption of no contact is invalid, and the sample will be reloaded. The average velocity of the sample face, under the action of the reverberating reflected pulse, is denoted $v_{1,ave}$. The reflection arrives at the sample face periodically at time intervals equal to the time needed to travel the length of the input bar twice. Each time the pulse acts at the sample face, it undergoes a displacement of

$$u_r^* = -2c_i \int \epsilon_r dt \tag{20}$$

where the factor of 2 is due to the free surface (assuming no contact), and the integral is performed over the entirety of the pulse. The average velocity is therefore
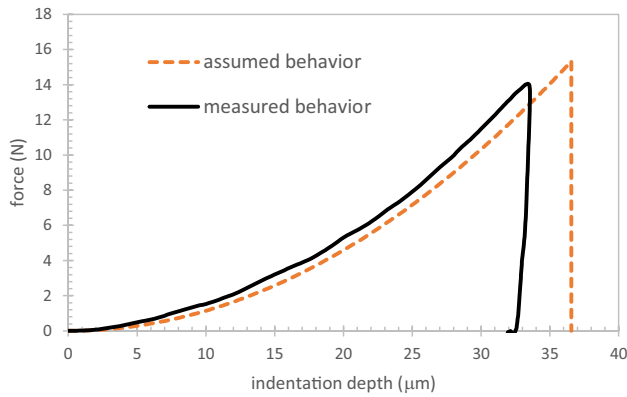
Fig. 14 The sample response assumed from an HV value of 434 GPa (orange). The actual response measured from the experiment (black, using Eq. (5) to measure v_1 in the calculation of indentation depth) (Color figure online)
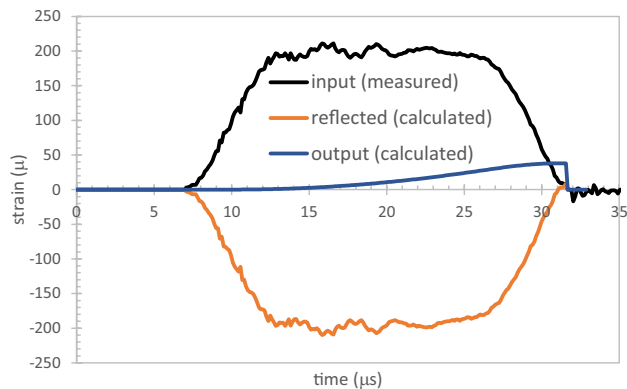

Fig. 15 The actual input pulse measured in the experiment (black) is used to predict the reflection and output pulse (Eqs. (14) and (15), respectively)

$$v_{1,ave} = \frac{u_r^*}{(2L_i/c_i)} = \frac{-c_i^2 \int \epsilon_r dt}{L_i} \tag{21}$$

Similarly, the average velocity of the indenter tip, assuming no further contact, is

$$v_{2,ave} = \frac{u_o^*}{(2L_o/c_o)} = \frac{c_o^2 \int \epsilon_o dt}{L_o} \tag{22}$$

Again, if $v_{2,ave} > v_{1,ave}$, natural recovery should occur.

An example application is now given using data from one of the experiments presented for copper in Figs. 4 and 5. Conventional hardness testing using loads of 1 kg-f yields HV = 434 GPa for this material. This value is used in Eq. (12) to estimate the mechanical response expected during the high-rate experiment; this is plotted with the dashed curve in Fig. 14. Since this experiment has already been conducted, the actual input pulse measured from the experiment can be used for ϵ_i to solve for ϵ_r and ϵ_o; these

are all plotted in Fig. 15. Figure 14 also shows the load vs indentation depth curve measured from this experiment. The difference between this and the assumed behavior is due mainly to the increase in HV at the higher loading rate, and the fact that a small gap (2 μm) existed between the sample and indenter tip prior to the experiment that is not accounted for in this analysis.

Equations (21) and (22) are next used to determine $v_{1,ave}$ and $v_{2,ave}$ as 0.12 and 0.19 m/s, respectively. $v_{2,ave}$ is considerably higher than $v_{1,ave}$, assuring natural recovery by a comfortable margin. It is also notable that this method estimates the final peak stress and maximum indentation depth in the experiment simply from the quasi-static HV value and the input pulse. This is another useful feature of this method for a wide range of Kolsky bar testing, and is further explained in the full analysis described in [22].

With a logical design of experiment, a single configuration can be used for a wide range of testing. For example, all the high-rate Vickers experiments in this document, over the complete loading range and for both materials, were performed with a single Kolsky bar arrangement; only the striker speed was varied between experiments. Natural recovery occurred in every case.

Declarations

Conflict of interest The authors have no relevant financial or non-financial interests to disclose.

References

1. ASTM-E10-18 (2018) Standard test method for Brinell Hardness of metallic materials. ASTM, West Conshohocken
2. ASTM C1326-13 (2018) Standard test method for Knoop indentation hardness of advanced ceramics. ASTM, West Conshohocken
3. ASTM C1327–15 (2019) Standard test method for Vickers indentation hardness of advanced ceramics. ASTM, West Conshohocken
4. Oliver W, Pharr G (2004) Measurement of hardness and elastic modulus by instrumented indentation: advances in understanding and refinements to methodology. J Mater Res 19(1):3–20
5. Pathak S, Kalidindi SR (2015) Spherical nanoindentation stress–strain curves. Mater Sci Eng R Rep 91:1–36
6. Fernandez-Zelaia P, Joseph VR, Kalidindi SR, Melkote SN (2018) Estimating mechanical properties from spherical indentation using Bayesian approaches. Mater Des 147:92–105
7. Sundararajan G, Shewmon P (1983) The use of dynamic impact experiments in the determination of the strain rate sensitivity of metals and alloys. Acta Metall 31(1):101–109
8. Marshall DB, Evans AG, Nisenholz Z (1983) Measurement of dynamic hardness by controlled sharp-projectile impact. J Am Ceram Soc 66(8):580–585
9. Tirupataiah Y, Sundararajan G (1991) A dynamic indentation technique for the characterization of the high strain rate plastic

flow behaviour of ductile metals and alloys. J Mech Phys Solids 39(2):243–271

10. Nobre J, Dias A, Gras R (1997) Resistance of a ductile steel surface to spherical normal impact indentation: use of a pendulum machine. Wear 211(2):226–236

11. Subhash G, Koeppel BJ, Chandra A (1999) Dynamic indentation hardness and rate sensitivity in metals. ASME J Eng Mater Technol 121:257–263

12. Koeppel BJ, Subhash G (1999) Characteristics of residual plastic zone under static and dynamic Vickers indentations. Wear 224:56–67

13. Nemat-Nasser S, Isaacs JB, Starrett JE (1894) Hopkinson techniques for dynamic recovery experiments. Proc R Soc A 1991(435):371–391

14. Casem DT, Pittari JJ III, Swab J (2021) High-rate indentation using miniature Kolsky bar methods. In: Mates S, Eliasson V, Allison P (eds) Dynamic behavior of materials, vol1. Conference proceedings of the society for experimental mechanics series. Springer, Cham

15. Casem DT, Grunschel SE, Schuster BE (2012) Normal and transverse displacement interferometers applied to small diameter Kolsky bars. Exp Mech 52(2):173–184

16. Avinadav C, Ashuach Y, Kreif R (2011) Interferometry-based Kolsky bar apparatus. Rev Sci Instrum 82:073908

17. Gorham DA (1983) A numerical method for the correction of dispersion in pressure bar signals. J Phys E Sci Instrum 16(6):477–479

18. Follansbee PS, Franz C (1983) Wave propagation in the split-Hopkinson pressure bar. J Eng Mater Technol 105:61

19. Gong JC, Malvern LE, Jenkins DA (1990) Dispersion investigation in the split-Hopkinson pressure bar. J Eng Mater Technol 112:309–314

20. Bancroft D (1941) The velocity of longitudinal waves in cylindrical bars. Phys Rev 59:588–593

21. Da Silva MG, Ramesh KT (1997) The rate-dependent deformation and localization of fully dense and porous Ti-6Al-4V. Mater Sci Eng A 232(1–2):11–22

22. Casem DT (2022) A model for a Kolsky bar experiment: application to experiment design, ARL-TR-9416

23. Bacon C (1994) Longitudinal impact of a shaped projectile on a Hopkinson Bar. J App Mech 61:493–495

24. Casem DT, Weerasooriya T, Walter TR (2018) Mechanical behavior of a low-cost Ti–6Al–4V alloy. J Dyn Behav Mater 4:138–149

25. Casem D (2022) Miniature Kolsky bar methods. In: Song B (ed) Advances in experimental impact mechanics. Elsevier, Amsterdam

26. Clayton J, Casem D, Lloyd J, Retzlaff E (2022) Toward material property extraction from dynamic spherical indentation experiments. Technical Report ARL-TR-9520; US Army Research Laboratory, Aberdeen Proving Ground: Adelphi

27. Clayton JD, Casem DT, Lloyd JT, Retzlaff EH (2023) Toward material property extraction from "dynamic spherical indentation experiments on hardening polycrystalline metals. Metals 13:276. https://doi.org/10.3390/met13020276

28. Clayton JD, Lloyd JT, Casem DT (2023) Simulation and dimensional analysis of instrumented dynamic spherical indentation of ductile metals. Int J Mech Sci 251:108333

29. Kalidindi SR, Pathak S (2008) Determination of the effective zero-point and the extraction of spherical nanoindentation stress-strain curve. Acta Mater 56(14):3523–3532

30. Oliver WC, Pharr GM (1992) An improved technique for determining hardness and elastic modulus using load and displacement sensing indentation experiments. J Mater Res 7(6):1564–1583

31. Strand OT, Goosman DR, Martinez C, Whitworth TL (2006) Compact system for high-speed velocimetry using heterodyne techniques. Rev Sci Instr 77:083108

32. Rosenberg Z, Kositski R, Ashuach Y, Leus V, Malka-Markovitz A (2019) On the upturn phenomenon in the strength vs. strain-rate relations of metals. Int J Solids Struct 176:185–190